J Mater Sci (2007) 42:5915–5923
DOI 10.1007/s10853-007-1772-x

Thermal property evolution of metal based thermal barrier coatings with heat treatments

Dong-Il Shin · François Gitzhofer · Christian Moreau

Received: 16 February 2006 / Accepted: 8 December 2006 / Published online: 19 May 2007

Abstract Predicting ''in-service'' lifetime of ceramic thermal barrier coatings (TBCs) is difficult due to the inherent brittle nature of ceramics used. Therefore, the study of metal-based thermal barrier coatings (MBTBCs) has been initiated to challenge the current problems of ceramic-based TBCs (CBTBCs) and create a new generation of thermal barrier coatings (TBCs). In this work, nano/amorphous structured MBTBCs, for use in internal combustion engines, have been produced using high frequency induction plasma spraying (IPS) of iron-based nanostructured alloy powders. Coatings were deposited by IPS using various spray parameters and heat treated up to 850 °C to study the thermal stability of the coating. The thermal diffusivity (α) properties of MBTBCs were measured using a laser flash method. Density (ρ) and specific heat (C_p) of the MBTBCs were also measured for calculating thermal conductivity ($k = \alpha\rho C_p$).

D.-I. Shin (✉)
Tekna Plasma Systems Inc., 2935 Boul Industriel, Sherbrooke, QC, Canada J1L 2T9
e-mail: Dong-il.Shin@Tekna.com

F. Gitzhofer
Centre de Recherche Energy, Plasma, and Electrochimique (CREPE), Department of Chemical Engineering, Université de Sherbrooke, Sherbrooke, QC, Canada J1K2R1

C. Moreau
Industrial Materials Institute, National Research Council of Canada, Boucherville, QC, Canada J4B6Y4

Introduction

Over the last two decades, thermal barrier coatings (TBCs) technologies have been improved enormously through the works of many researchers. Yttria stabilized zirconia (YSZ) has been widely studied as a thermal insulator at elevated temperatures since it has one of the lowest thermal conductivities (TC) (about 2 W/mK as a bulk material), along with one of the highest expansion coefficients for a ceramic material (9.5×10^{-6}/K), close to those of some metals [1]. Thermal spraying is commonly used to deposit YSZ coatings, to protect and insulate the hot section metal components of advanced gas-turbines or diesel engines. Thermally sprayed YSZ as TBCs achieves TC values of less than 1 W/mK [2]. Doping YSZ or Hf-Y_2O_3 with multi-component oxides have shown further reductions in thermal conductivity of 50–60% and improved thermal stability associated with the paired rare earth dopant additions and defect cluster formation [3].

The use of TBCs can result in a temperature reduction of as much as 200 °C at the metal surface, thereby improving the durability of metal components as well as enhancing the fuel efficiency [4]. However, TBCs using the traditionally employed ceramic materials, such as YSZ, have poor reliability due to their inherent brittle behavior of the ceramic making lifetime prediction difficult. Therefore, a new concept of metal-based TBCs (MBTBCs) has been devised and is now considered for a new generation of TBCs.

For the MBTBCs, it is very important to consider the free electron contributions to thermal conductivity because most of the metallic based materials are electrically and thermally conductive due to the existence of free electrons and phonons propagation at the atomic scale. The basic relationship between thermal conductivity (k) and a

corresponding mean free path (ℓ), for either electrons or phonons, can be defined as $k = \frac{1}{3}Cv\ell$ [1].

Thermal conductivity, k, can be minimized by reducing the mean free path. One of approach is to the reduce ℓ by engineering scatterings defects into the material to hinder the mobility of electrons or phonons. Imperfections must be tailored to the type of scattering required. For instance, high frequency phonons, which have wavelengths of the order of atomic dimensions, are scattered by point defects, while grain boundaries scatter low frequency phonons with phonon mean free paths comparable to the material grain size [5–7]. This was demonstrated by Yang et al. [8] who reported that a strong, grain-size-dependence of thermal conductivity from 6 to 480 K for YSZ. They reported YSZ with a 10 nm grain size has a thermal conductivity less than half that of much coarser-grained (micron scaled) coatings [8].

The present work extends the concepts of fine grain size and the use of scattering centers to the reduction of thermal conductivity of metal-based thermal barrier coatings.

Description of experiments

Coating production

In this work, MBTBCs were plasma-sprayed from iron based alloy powders using induction plasma spraying (IPS) [9, 10] and air plasma spaying (APS). The powder used is a commercially available iron based alloy material. The thermal conductivity of the coatings ''as-sprayed'' and heat treated was calculated, from measurement of the density (ρ), specific heat (C_p), and thermal diffusivity (α). Crystal structure and phase changes in MBTBCs before and after heat treatment (HT) were characterized by transmission electron microscopy (TEM) and X-ray diffraction (XRD).

The coatings were deposited by injecting the starting powder into Ar-N_2 (IPS-N_2) or Ar-O_2 (IPS-O_2) plasma, formed using a high frequency induction plasma torch (PL-50, TEKNA Plasma System, Inc.). The starting powder (SHS717, Nanosteel Co.) has a composition of Fe–25Cr–8Mo–10W–5Mn–5B–2C–2Si in wt.% and low thermal conductivity as 5–6 W/mK [11]. The particle size distribution of the starting powder was $d_{10\%}$ = 17 μm, $d_{50\%}$ = 23 μm, and $d_{90\%}$ = 45 μm. SEM images of the powder in as-received condition are presented in Fig. 1. In the SEM micrographs, it is noticed that nanostructured features in the size range of 50–150 nm are observable in the cross-section of individual powder grains. IPS parameters were optimized to reach the lowest thermal conductivity of the MBTBCs. The optimization of IPS parameters was performed using a factorial design of experiment and the results were assessed by analysis of variance (ANOVA) [12], and the optimized IPS parameters are presented in Table 1.

For comparison air plasma spraying (APS) was also used for preparation of a series of MBTBC samples due to its general and commercial use in industry. One set of APS spray conditions, adopted from the work done by Rohan [13], was used in this study. This will enable a comparison between APS MBTBCs and IPS MBTBCs. APS parameters were not optimized for any desired thermal properties of the coatings in this study. During the IPS deposition, the coating temperature was indirectly measured by measuring the substrate temperature using a temperature indicating

Table 1 IPS spraying conditions

Parameters		IPS-N_2	IPS-O_2
Power (kW)		24	
Feedrate (g/min)		16	
Substrate cooling		Water	
Coating temperature controlled with		Liquid N_2	
Chamber pressure (Torr)		100	
Spraying distance (mm)		210	
Gas flow (slpm)	Ar-sheath	62	45
	Sheath	20 (N_2)	37 (O_2)
	Ar-central	23	
	Ar-carrier	4	

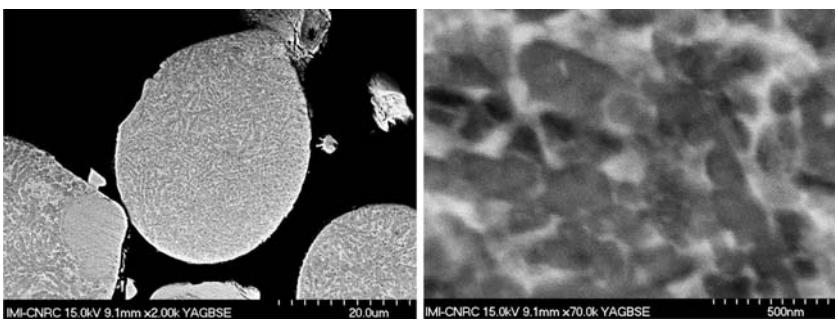

Fig. 1 SEM images on a cross-section of SHS717 powder in as-received condition

lacquer (OMEGALAQ ® Liquid), and it showed that the substrate temperature was kept under 200 °C.

YSZ coatings were also produced by APS for comparison with the MBTBCs.

Coating characterization

In order to understand the microstructure and phase stability of coating thermal properties, coatings were selected from each IPS-N_2 and IPS-O_2 deposition process [12] and heat treated at five different temperatures, 450, 550, 650, 750, and 850 °C, for 1 h under an Ar atmosphere. As the coatings are heat treated at different temperatures, microstructure changes of the coatings, such as porosity, grain growth, recrystallization, and phase precipitation were expected to take place. Changes in the thermal properties of each coating was measured as a function of heat treatment temperature.

The X-ray diffraction technique was used for phase identification and grain size measurement of the coatings (Philips X'pert Pro MPD). The Scherrer equation was used to estimate the average grain size in the sprayed coatings, using the full width at half maximum (FWHM) values obtained from the XRD patterns of the coatings [14, 15].

Scanning electron microscopy (SEM, JEOL JSM-840A/Hitachi S4700 Cold Field Emission) was used to observe coating's structure and porosity in backscattered electron mode on micropolished cross-sections of the coatings. Transmission electron microscopy (TEM, JEOL JEM 2100M) was used to observe the crystal structure and nanostructured grain sizes. Samples were sliced into the dimensions of 10 μm (W) × 8 μm (L) × 200 nm (T) using a focused ion beam system (FIB, Hitachi FB2000A). The identified crystal structure and gain size as measured by TEM diffraction technique and image analysis, respectively, are used to confirm the data from the XRD measurements.

Coating porosity was measured by image analysis with five randomly taken SEM pictures from each sample at 500× magnification. The apparent density (DN) of the sprayed coatings was measured by the Archimedes principle [16]. Thermal diffusivity (TD) measurement of the coatings was carried out at room temperature by using the laser flash method [17]. A 0.8 J YAG laser pulse (70 μs duration, 6 mm diameter) was used to heat the front coating surface, and the temperature of the rear surface was monitored using an infrared InSb detector. The infrared signal was digitized using a Nicolet 440 scope. Coatings were detached from their substrate before TD measurement. Specific heat (C_p) of the coatings was also measured using the Q1000 Tzero^{TM} DSC (Differential scanning calorimetry, TA Instruments, Delaware, USA) at room temperature. Thermal conductivity (k) was calculated by use of the relationship $k = \alpha\rho C_p$.

To quantify the empirical electron/phonon contribution to the thermal transport properties, the electronic thermal conductivity (k_e) of each sample was calculated from measured electric conductivity with a four point probe method using the Wiedemann-Franz law, which is written in Eq. 1 [18]. As presented in the Eq. 2, subtracting k_e from the measured thermal conductivity, $k = \alpha\rho C_p$, yields a thermal conductivity portion by the phonon contribution. Therefore, the phonon thermal conductivity, k_P, in alloys can be deduced using the expression set out below

$$\frac{k_e}{\sigma} = 3\left(\frac{k_B}{e}\right)^2 T \tag{1}$$

$$k_P = k - k_e = \alpha\rho C_p - 3\sigma\left(\frac{k_B}{e}\right)^2 T \tag{2}$$

where k_B, is the Boltzmann constant, e is electronic charge, σ is electrical conductivity, and T is temperature at measurement.

Since plasma-sprayed coatings have an anisotropic structure, two different incident directions of the laser beam were used to study the corresponding anisotropy in their thermal diffusivity, as shown in Fig. 2. The laser incident direction was either parallel (PA) or perpendicular (PE) to the spray direction as indicated by the dotted arrows in Fig. 2. The measurement in the PE direction was carried out on a slice cut from a 1 cm thick coating.

Results and discussion

Evolution on MBTBCs' properties with heat treatments

The XRD patterns of the IPS-N_2 and APS deposited MBTBCs are presented as a function of HT temperature in Fig. 3. The coating structure changes from amorphous to crystalline with new phases precipitating at 550 °C. The phases precipitated

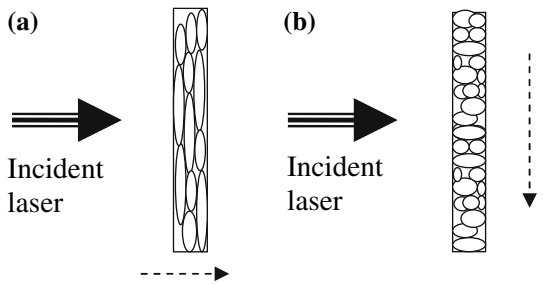

Fig. 2 Thermal diffusivity measurements (**a**) PA direction: the incident laser is parallel to spraying direction, (**b**) PE direction: the incident laser is perpendicular to the spraying direction. The *dotted arrows* indicate the spraying direction

are identified as Fe or Cr based alloys such as $Fe_{23}(C,B)_6$ or $Cr_{23}C_6$. These alloy materials are highly conductive materials—their thermal conductivities are known as Fe based alloy about 80 W/mK and Cr based alloy about 94 W/mK, [19]. Both IPS and APS have similar phase precipitation, except for magnetite (Fe_3O_4) found in APS.

SEM micrographs in Fig. 4 show that APS coatings have better interlamellar contacts between splats than IPS-N_2 coatings. The coating structure is not significantly affected by HT for the IPS-N_2 samples for all temperatures while some densification is observed for the APS samples.

Grain size measurements, by the XRD with Scherrer equation techniques and image analysis on TEM micrographs, were performed. The grain size change along the heat treatment temperature increase is presented in Fig. 5. Coatings as-sprayed and after heat treatment at 450 °C have grain sizes (of around) from 3 to 4 nm, implying that they are most likely amorphous. Following a HT at 550 °C, the grain size of the MBTBCs was increased, by more than 10 times. The grain size calculated by the Scherrer method for APS and IPS-N_2 MBTBCs, with HT at 850 °C, was 40–50 nm. However, TEM (transmission electron microscopy) images presented in Fig. 6 show that grain sizes of the APS and IPS-N_2 MBTBCs after the HT at 850 °C are of the order of 200 nm, having been changed from an initial size of around 20 nm (after the HT at 550 °C). The difference lies in the range of validity of the Scherrer equation. If the grain size is greater than ~150 nm, the Scherrer equation is difficult to apply due to the lack of sensibility of the technique [14]. Therefore, in Fig. 5, the grain size values up to heat treatment temperature of 650 °C were measured by Scherrer equation, and others by image analysis.

Figure 7 shows porosity changes in heat treated MBTBCs. One noticeable result is that there is little porosity change with heat treatment (HT) of IPS MBTBCs, but the porosity of APS with the HT at 850 °C decreased by about 4%. As shown in Fig. 8, no significant density changes occur with the HT. The slight density drop in APS MBTBCs with HT at 750 and 850 °C cannot therefore be explained by the porosity change. It is more likely associated with precipitation of a new phase in the coatings at elevated temperatures. However, the lower density of APS MBTBCs, compared to IPS MBTBCs, can be explained by the lower density iron oxides, such as Fe_3O_4, that the APS MBTBCs contain.

Precipitated grains, as displayed in Fig. 6, were analyzed by the EDS (energy dispersive spectroscopy) mapping technique, as shown in Fig. 9. From the results of this mapping, the white grains were identified as W and Mo rich phases, and the gray/black grains were identified as Fe rich phases.

Thermal diffusivity (TD) measurements show that APS MBTBCs do have higher TD values than IPS MBTBCs at all HT temperature ranges, as shown in Fig. 10. One has to keep in mind that the APS coatings were not optimized for lower thermal conductivity, contrary to the efforts made for the IPS coatings. Lower TD values of APS coatings could possibly be reached after proper optimization. A general increase in the TD with HT is noted at 550 °C for all types of MBTBCs. A second increment of TD was observed in APS MBTBCs after HT above 750 °C, while no more change was observed in the IPS MBTBCs. These increases may be associated with three factors: crystal structure, grain size, and phase changes.

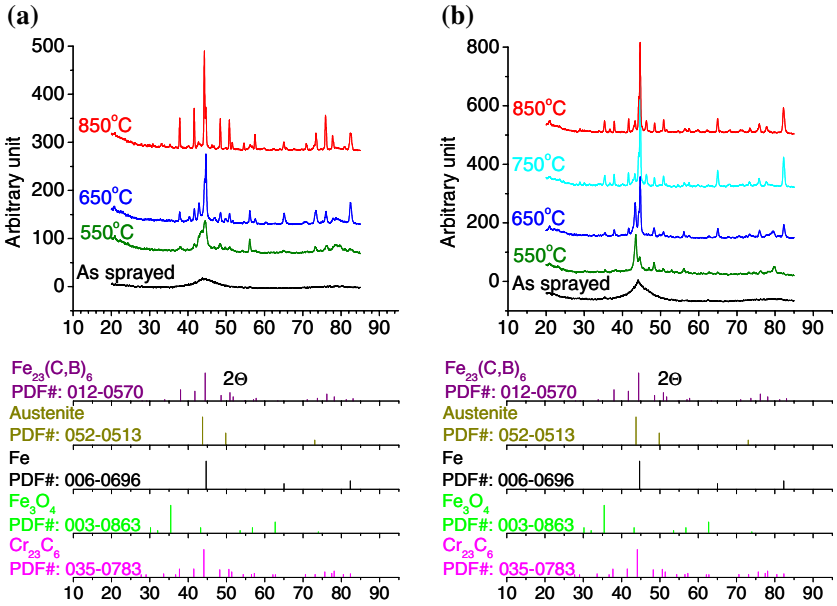

Fig. 3 X-ray Diffraction Pattern changes of; (**a**) IPS-N_2 and (**b**) APS MBTBCs as-sprayed and after heat treatment; all PDF data are from Ref. [18]

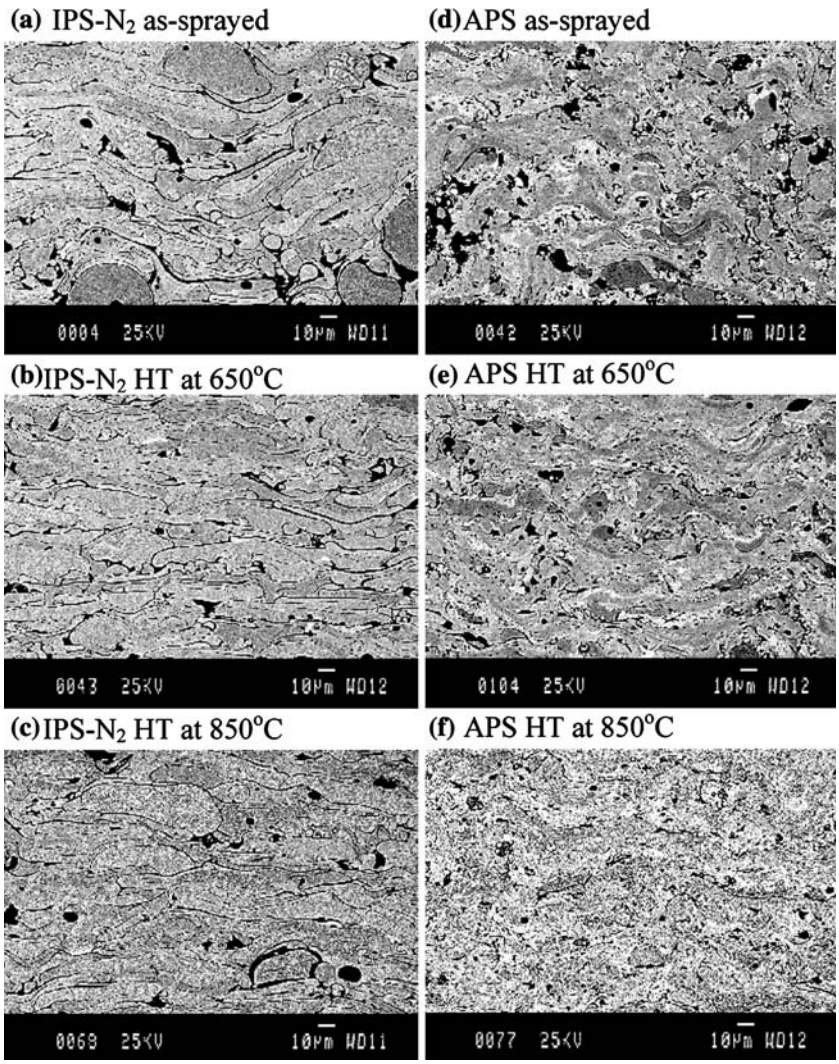

Fig. 4 Backscattered SEM images of heat treated MBTBCs, (**a**–**c**) IPS and (**d**–**f**) APS

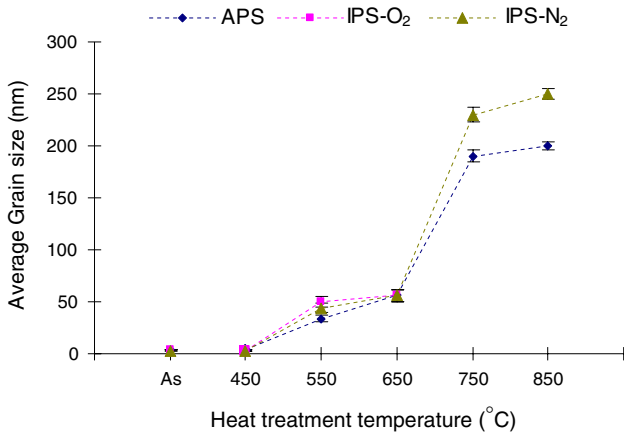

Fig. 5 Grain size changes in MBTBCs with heat treatment for 1 h under Ar; grain size up to 650 °C were determined by Scherrer equation, and the size at 750 and 850 °C were measured by image analysis on TEM pictures

Two factors, crystal structure change and grain size increase, seem to be associated with the TD increase after HT at 550 °C. As shown in Fig. 3, crystal structure changed from amorphous to crystalline, and grain size also increase from a few nanometers to tens of nanometers, as presented in Fig. 5. However, TD looks independent of the grain size in IPS-N_2 MBTBCs because TD values remain within the error range while grain size changes from 60 to 150 nm after HT at 750 °C. In case of APS MBTBCs, there is another TD value shift observed after HT at 750 °C. The TD increase can be explained by the precipitation and growth of a new phase in the coatings. As seen in Fig. 3, the content of Fe_3O_4 phase in APS MBTBCs gets maximized after HT at 750 °C. Since thermal conductivity of magnetite is known as 9.7 W/mK [20], it appears likely that the Fe_3O_4 rich phase, present in APS MBTBCs, is responsible for the TD increase after HT at 750 °C.

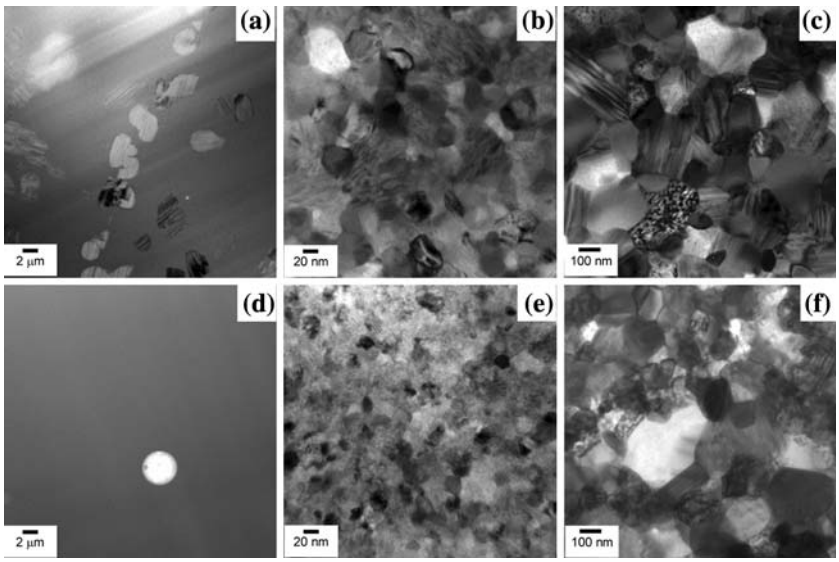

Fig. 6 TEM images of IPS-N_2 MBTBCs, (**a**) as-sprayed, (**b**) HT at 650 °C, (**c**) 850 °C, and APS MBTBCs, (**d**) as-sprayed, (**e**) HT at 550 °C, (**f**) 850 °C

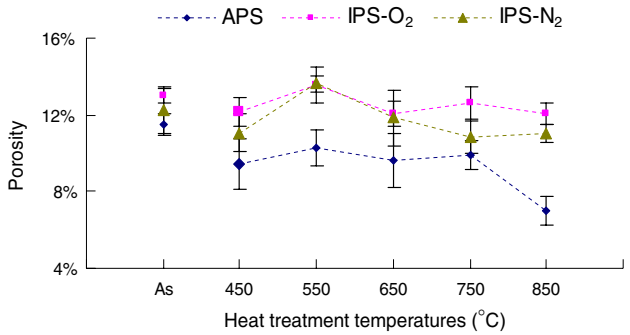

Fig. 7 Porosity changes in as-sprayed and heat treated MBTBCs

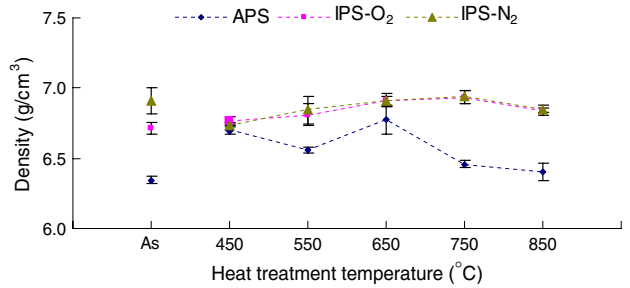

Fig. 8 Density changes in as-sprayed and heat treated MBTBCs

Decrease of interlamellar porosity may also participate in the observed TD increase.

Thermal conductivity of MBTBCs

Thermal conductivities of MBTBCs and plasma sprayed YSZ were calculated and presented in Table 2. Comparing APS-MBTBCs with IPS MBTBCs, their density is lower and their heat capacity is higher. The lower density is due to the presence of oxide phase, while the higher heat capacity can be explained by the higher oxygen wt.% in these coatings. The nitrogen wt.% in coatings does not affect significantly the properties, while the oxygen wt.% affects to them as shown in Fig. 11.

The lowest thermal conductivity (TC) found for MBTBCs is 2.0 W/mK, while the TC of plasma sprayed YSZ is 1.2 W/mK. As noted about the thermal diffusivity measurements, the higher TC values of APS and IPS-O_2, compared to those of IPS-N_2 MBTBCs likely results from the presence of Fe_3O_4.

It is worth noting that, in all industrial applications, YSZ-TBCs are always deposited on a metallic bond-coat (BC) in order to obtain a good bond between the ceramic layer and the substrate. Typically, a 300-μm thick YSZ layer is deposited on a 150-μm BC whose thermal conductivity is around 4.2 W/mK [21]. The calculated thermal resistance of a 450-μm thick IPS-N_2 MBTBCs is 2.25×10^{-4} m^2 K/W which is 21% lower than the thermal resistance (2.85×10^{-4} m^2 K/W) provided by the typical YSZ TBC system mentioned above. The actual thermal resistance values of YSZ + BC duplex are measured published elsewhere [22], as in the range of 2–3.5 × 10^{-4} m^2 K/W.

Table 3 shows theoretically predicted TC values of MBTBCs, using the ''rule of mixtures'' approach[1] with respect to Fe_3O_4 wt.% present in the coating. The wt.% of Fe_3O_4 in MBTBCs is calculated from the O_2 wt.% in MBTBCs, assuming conversion of the all O_2 fraction to Fe_3O_4 without taking account on possibility of oxygen

[1] A Rule of Mixture $TC_{Total} = TC_{Fe_3O_4}WF_{Fe_3O_4} + TC_{MBTBCs}WF_{MBTBCs}$; $TC_{Fe_3O_4}$ and TCMBTBCs are the thermal conductivity of Fe_3O_4 (=9.7 W/mK) and IPS-N2 MBTBCs as-sprayed (=1.99 W/mK); $WF_{Fe_3O_4}$ and WF_{MBTBCs} are the percentages (fractions) of Fe_3O_4 and IPS-N2 MBTBCs as-sprayed, respectively.

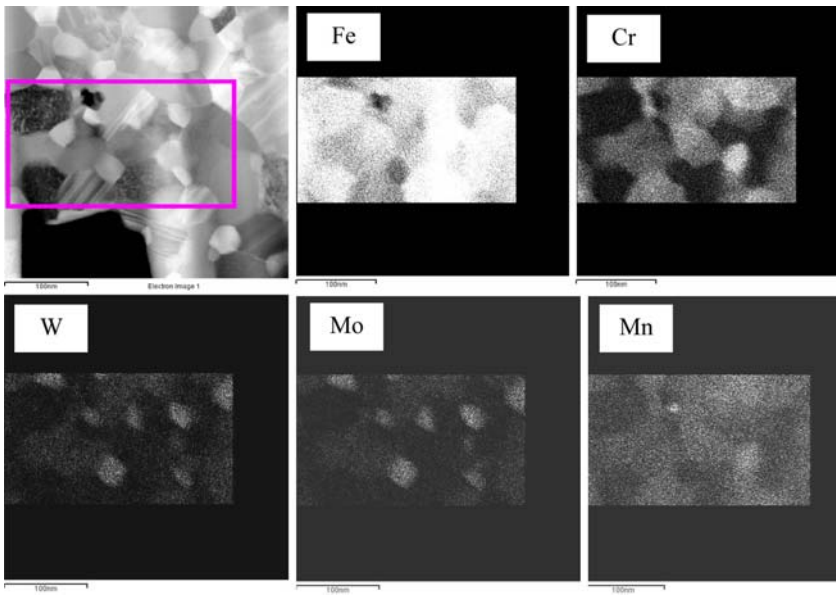

Fig. 9 Results of EDS mapping for component analysis on IPS-N_2 MBTBCs after HT at 850 °C

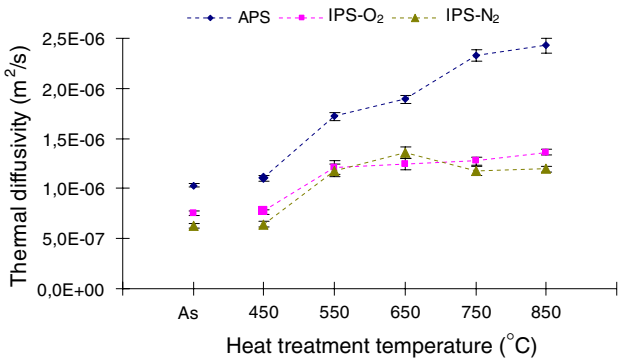

Fig. 10 Thermal diffusivity changes in as-sprayed and heat treated MBTBCs

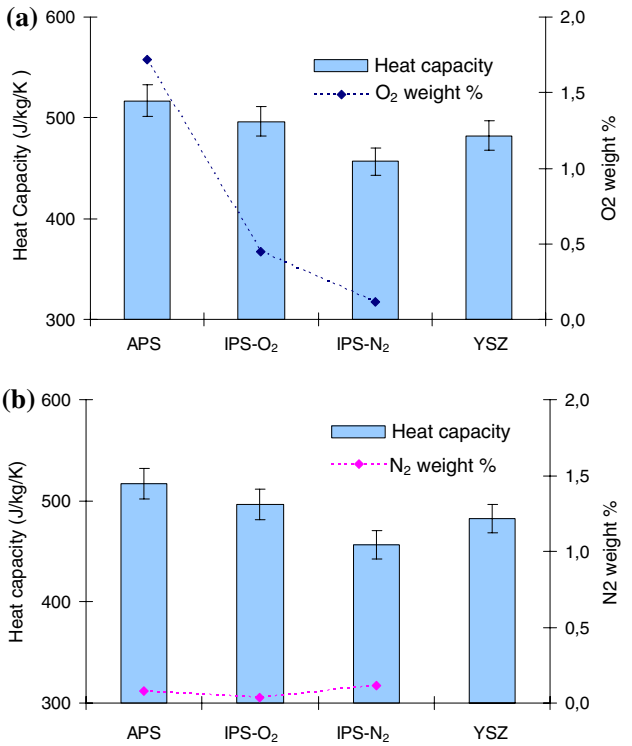

Fig. 11 Heat capacity changes in as-sprayed MBTBCs and as-sprayed YSZ with; (**a**) oxygen contents, and (**b**) nitrogen contents

solution in Fe due to its low solubility (0.001% at 912 °C) [23]. The results show that the actual TC values measured for APS and IPS-O_2 MBTBCs, as presented in Table 2, is higher than those predicted in Table 3, which means that Fe_3O_4 is not the only factor in accounting for the higher TC in APS and IPS-O_2 MBTBCs but that other factors are also associated.

As shown in Fig. 12, the phonon contribution is dominant in APS MBTBCs, while the electron contribution becomes the dominant factor for the total TC in IPS-N_2 MBTBCs.

Table 2 Thermal conductivity of MBTBCs and plasma sprayed YSZ

Sample ID	TD (10^{-6} m^2/s)	Density (kg/m^3)	C_p (J/kg/K)	TC (W/m/K)	Porosity (%)
APS	1.03 ± 0.02	6,350 ± 25	520 ± 10	3.4 ± 0.1	12 ± 0.5
IPS-O_2	0.75 ± 0.02	6,720 ± 50	500 ± 10	2.5 ± 0.1	13 ± 0.4
IPS-N_2	0.63 ± 0.02	6,910 ± 100	460 ± 10	2.0 ± 0.1	12 ± 1.3
YSZ	0.49 ± 0.02	4,950 ± 25	490 ± 10	1.2 ± 0.1	10 ± 2.0

Table 3 Thermal conductivity of MBTBCs with respect to Fe_3O_4 wt.%

Sample ID	Fe_3O_4 (wt.%)	IPS-MBTBCs (wt.%)	Predicted TC (W/mK)
APS	0.86	99.14	2.05
IPS-O_2	0.22	99.78	2.00
IPS-N_2	0.06	99.94	1.99

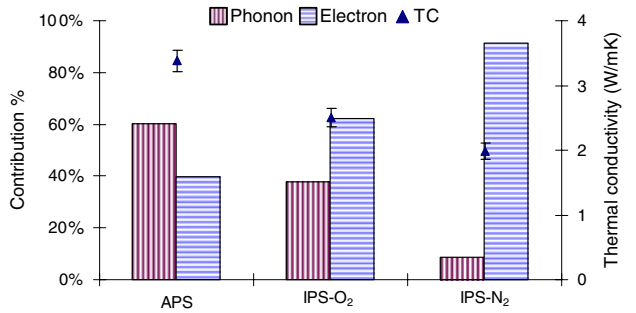

Fig. 12 Phonon and electron contributions to thermal conductivity of MBTBCs as-sprayed

Anisotropic effects on the thermal conductivity are not very significant and are neglected in this study. As presented in Figs. 13, 14, IPS-N_2 MBTBCs consist of an amorphous crystal structure, while APS MBTBCs consist of partially ordered atoms in an amorphous structure. The lower phonon contribution to the total TC in IPS-N_2 MBTBCs as compared to other MBTBCs is attributed to this amorphous structure. The lower thermal diffusivity and conductivity of alloys with amorphous structures are published elsewhere [24, 25]. The work of Yamasaki has reported that amorphous metals exhibit more than 50% lower thermal diffusivity and conductivity than for crystalline metals in Zr-based alloys. Harms [25] has also presented the point that thermal conductivity (TC) of Pd-based metallic glass alloys is less than 2 W/mK. The author explains that the phonon contribution to the total TC is certainly limited in metallic glass materials, and then only the electronic contribution becomes the dominant factor for the TC. This explanation is in agreement with the understanding of the low thermal conductivity of amorphous MBTBCs in this study.

Conclusions

The concept of metal-based thermal barrier coatings (MBTBCs) is presented and demonstrated using induction plasma spraying (IPS) iron based, nanostructured alloy powders. The concept was initiated to develop a new generation of TBCs with enhanced mechanical properties

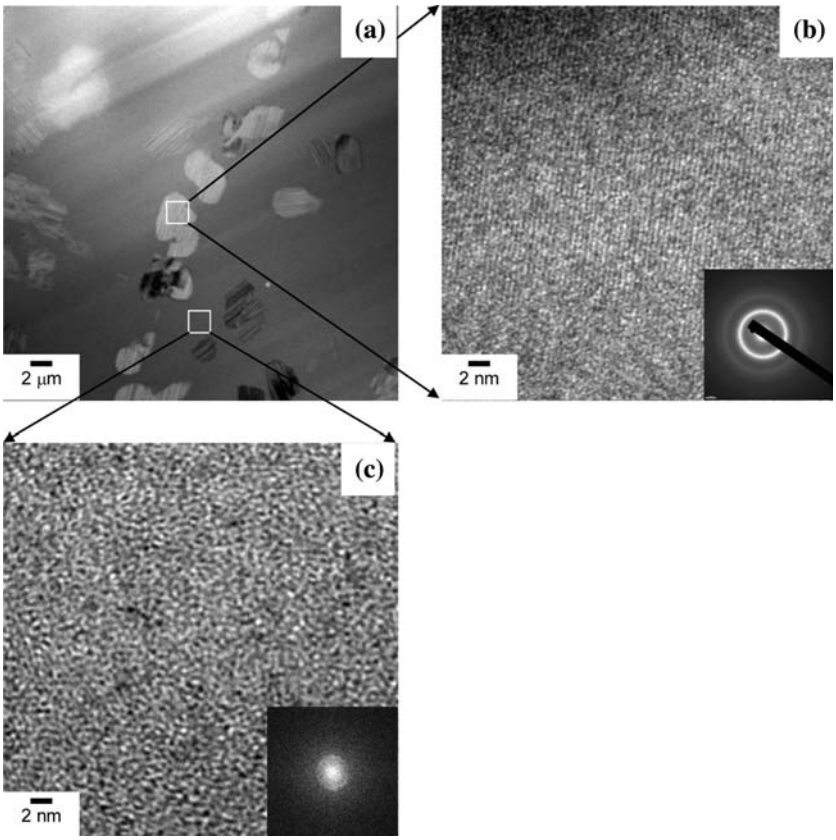

Fig. 13 TEM images on as-sprayed MBTBCs with IPS-20% N_2 and SD of 150 mm, (**b**) and (**c**) are high resolution images of the ''square'' sampled areas indicated in the image (**a**)

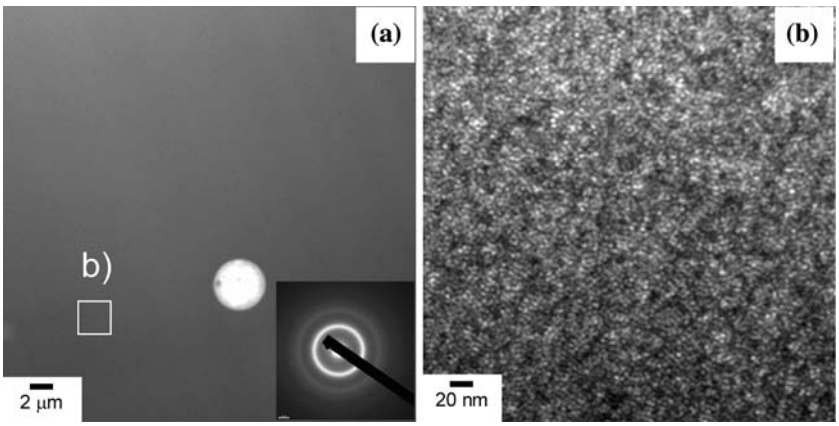

Fig. 14 TEM micrographs of as-sprayed APS MBTBCs; (**a**) with its diffraction pattern, and (**b**) with high resolution on white squared area in the image of (**a**)

of metallic based materials, thus differentiating them from current ceramic-based TBCs (CBTBCs).

The main experimental values obtained from this work are listed below:

1. Amorphous structured MBTBCs were produced by using thermal plasma spraying of iron based nano-structured alloy powders.
2. Thermal diffusivity (TD) of the amorphous MBTBCs doubles when the crystal structure changes from amorphous to crystalline accompanying with phase precipitations after heat treatment at 550 °C for 1 h under argon atmosphere.
3. The lowest thermal conductivity (TC) of the amorphous MBTBCs, calculated from their TD values, is 2.0 W/mK. The TC is dominated by the electronic contribution; the phonon contribution is relatively small in MBTBCs due to the amorphous structure.
4. The low TC was obtained because of the increased phonon scattering by the amorphous structure in the coatings so that the phonon contribution to TC was suppressed.

In summary, we may conclude that thermal properties of MBTBCs are mainly governed by *two* factors, such as (1) phases and (2) crystal structure (amorphous or crystalline). There are also hidden factors, such as interlamellar contact, splat thickness, the ratio between molten/unmolten numbers of particles in the coatings, and crack lengths, which should be considered to complete the correlation between the dependent and independent variables.

References

1. Kingery WD, Bowen HK, Uhlmann DR (1976) Introduction to ceramics, 2nd edn. John Wiley and Sons, New York, p. 595
2. Slifka AJ, Filla BJ, Phelps JM, Bancke G, Berndt CC (1998) J Thermal Spray Technol 7(1):43
3. Zhu D (U.S. Army Research Laboratory), Miller RA (2004) Thermal and environmental barrier coatings for advanced propulsion engine systems. Annual forum proceedings – American Helicopter Society, vol 1, 60th Annual forum proceedings – American Helicopter Society, pp 703–709
4. Schlichting KW, Padture NP, Klemens PG (2001) J Mater Sci 36:3003
5. Kumar S, Vradis GC (1994) Trans ASME 116:28
6. Klemens PG (1997) Theory of thermal conductivity of nano-phase materials, chemistry and physics of nanostructures and related non-equilibrium materials. Warrendale, PA, USA, pp 97–104
7. Raghavan S, Wang H, Dinwiddie RB, Porter WD, Mayo MJ (1998) Scripta Mater 39(8):1119
8. Yang H-S, Eastman JA, Thomson LJ, Bai GR (2002) Mater Res Soc Symp Proc 703:179
9. Shin D, Gitzhofer F, Moreau C (2004) In: Proceedings of ITSC 2004, May 2004, Osaka, The nanostructure material section
10. Shin D, Gitzhofer F, Moreau C (2005) In: Proceedings of ITSC 2005, May 2–3, Basel, Swiss
11. Branagan DJ, Swank WD, Haggard DC, Fincke JR (2001) Metall Mater Trans A 32A:2615
12. Shin D-I, Gitzhofer F, Moreau C (2007) J Thermal Spray Technol 16(1):118
13. Rohan P, Bouaricha S, Legoux J-G, Moreau C, Ctibor P, Nourouzi S, Vardelle A (2004) In: Proceedings of ITSC 2004, May 2004, Osaka, Japan
14. Klug HP, Alexander LE (1974) X-ray diffraction procedures, 2nd edn. John Wiley & Sons, NY, USA
15. Cullity BD (1990) Elements of X-ray diffraction, 2nd edn. in Korean Version. Bando Publishing Co. Ltd, Korea (translated by B.H. Han)
16. Haraguchi T, Yoshimi K, Kato H, Hanada S, Inoue A (2003) Intermetallics 11:707
17. Parker WJ, Jenkins RJ, Butler CP, Abbott GL (1961) J Appl Phys 32(9):1679
18. Hook J, Hall H (1991) Solid state physics, 2nd edn. John Wiley and Son
19. Kittel C (1996) Introduction to solid state physics, 7th edn. John & Wiley Inc, Chichester
20. CES Selector 4.1, Granta Design Limited, Rustat House, 62 Clifton Road, Cambridge, CB1 7EG, UK
21. Khor KA, Gu YW (2000) Thin Solid Films 372:104
22. Gitzhofer F, Pawlowski L, Lombard D, Martin C, Kaczmarek R, Boulos M (1985) High Temp – High Pres 17(5):563
23. Wriedt HA (1990) In: Massalski TB (ed) Binary alloy phase diagrams, 2nd edn. ASM International, Materials Park, OH, pp 1739–1744
24. Yamasaki M, Kagao S, Kawamura Y, Yoshimura K (2004) Appl Phys Lett 84(23):4653
25. Harms U, Shen TD, Schwarz RB (2002) Scripta Mater 47:411